Revealing the atomic and electronic structure of a SrTiO3/LaNiO3/SrTiO3 heterostructure interface

Zaoli Zhang, S. Soltan, H. Schmid, H.-U. Habermeier, B. Keimer, and U. Kaiser

Citation: Journal of Applied Physics **115**, 103519 (2014); doi: 10.1063/1.4868513
View online: http://dx.doi.org/10.1063/1.4868513
View Table of Contents: http://scitation.aip.org/content/aip/journal/jap/115/10?ver=pdfcov
Published by the AIP Publishing

Revealing the atomic and electronic structure of a $SrTiO_3/LaNiO_3/SrTiO_3$ heterostructure interface

Zaoli Zhang,[1,2,a)] S. Soltan,[3,4] H. Schmid,[5] H.-U. Habermeier,[3] B. Keimer,[3] and U. Kaiser[2]
[1]*Erich Schmid Institute of Materials Science, Austrian Academy of Sciences, Leoben, Austria*
[2]*Electron Microscopy Group for Materials Science, University of Ulm, Ulm, Germany*
[3]*Max-Planck Institute for Solid State Research, D-70561 Stuttgart, Germany*
[4]*Faculty of Science, Helwan University, 11795 Cairo, Egypt*
[5]*INM—Leibniz-Institut für Neue Materialien, 66123 Saarbrücken, Germany*

(Received 12 December 2013; accepted 1 February 2014; published online 14 March 2014)

The atomic structures of $SrTiO_3$ (STO)/$LaNiO_3$ (LNO)/STO heterostructure interfaces were investigated by spherical aberration-corrected (C_S) (scanning) transmission electron microscopy. Atomic displacement and lattice distortion measurements and electron energy loss spectroscopy (EELS) were used to quantitatively analyze the distortion of the interfacial octahedra and the bond length at the interfaces. Combined with high-resolution transmission electron microscopy (HRTEM) and scanning transmission electron microscopy analyses, two distinct interfacial atomic terminating layers are unambiguously determined. Ensuing quantitative HRTEM measurements revealed that the Ni-O bond length in the interfacial octahedral is elongated at the bottom interface (–NiO_2-SrO–). Atomic displacement shows structural relaxation effects when crossing the interfaces and lattice distortions across the interface is more pronounced in LNO than in STO. The Ti/O atomic ratio, La and Ti relative atomic ratio as derived by EELS quantification indicate non-stoichiometric composition at the interfaces. Distinct fine structures of Ti-$L_{2,3}$ edge and O-K edge at the bottom and top interfaces are observed. By comparison, we are able to estimate Ti valency at both interfaces. Combining the structural distortions and Ti valency, the polar discontinuity and charge transfer at the interfaces are discussed. © *2014 AIP Publishing LLC*.
[http://dx.doi.org/10.1063/1.4868513]

I. INTRODUCTION

The interplay between the lattice structure and electronic properties in transition metal oxides (TMOs) has been studied extensively during the past three decades.[1] Most TMOs crystallize in the perovskite structure or its derivatives, which is built up of MO_6 octahedra. Theories of the electronic system in TMOs require detailed experimental information about the arrangement of these octahedra, which can be gleaned from X-ray and neutron diffraction data. The M-O bond lengths within the octahedra yield information about the valence state of the transition metal ions. Bond length distortions control the orbital degeneracy of the transition metal ion at its center via the Jahn-Teller effect, which also crucially affects the electronic properties of TMOs. The transition relative orientation of the octahedra, which is determined by steric constraints in the perovskite structure, influences the M-O-M bond angle and hence the magnitude of the inter-site electron transfer, which in turn controls the sign and magnitude of magnetic exchange interactions in Mott insulators or the conduction electron bandwidth in metals. Motivated by the discovery of interfacial electronic systems with high mobility in TMO heterostructures and the prospect of device applications,[2] the electronic structure of TMO interfaces has recently taken center stage in solid-state physics. In view of the lessons learnt from research on bulk TMOs, one again expects a crucial influence of the size, shape, and orientation of the MO_6 octahedra on the electronic properties of these interfaces. While x-ray and neutron diffraction can be applied to determine the average structural properties of thin films, they are not generally applicable as probes of interfacial structures that lack translational periodicity (with the exception of very thin overlayers, see Ref. 3). Fortunately, high-resolution transmission electron microscopy (HRTEM) and scanning TEM (STEM) have developed into powerful probes of the local structure of TMO interfaces, following the advent of spherical aberration (C_S) correctors that greatly enhance the point resolution.[4] Such experiments have yielded detailed information about the atomic stacking sequences at various heterointerfaces and atomic displacements including distortions of the MO_6 octahedra.[5,6] In combination with electron energy-loss spectroscopy, information about the valence states of interfacial ions and intermixing of different ionic species has also been derived from TEM data.

We have applied C_S-corrected HRTEM and STEM to a trilayer heterostructure composed of a ~30 nm thick $LaNiO_3$ (LNO) layer grown on a $SrTiO_3$ (STO) substrate and a STO capping layer. Bulk perovskites of composition $RNiO_3$, where R denotes La^{3+} or a trivalent rare-earth cation, have been extensively studied in view of bandwidth-controlled metal-insulator transitions driven by modifications of the Ni-O-Ni bond angle via external pressure or the size of the R^{3+} ions.[1] While most $RNiO_3$ compounds exhibit insulating

a)Author to whom correspondence should be addressed. Electronic mail: zaoli.zhang@oeaw.ac.at

states with charge and spin order at low temperatures, bulk LNO remains metallic at all temperatures. This has stimulated several studies on LNO thin films and heterostructures that addressed the influence of epitaxial strain and layer thickness on the phase behavior of this system. Predictions of superconductivity[7,8] and multiferroicity[9] in LNO heterostructures have provided further motivation for these studies. While these predictions have thus far not been confirmed, the electrical conductance through thin LNO layers was reported to depend strongly on their thickness.[10–12] The crystalline quality of LNO film could influence electrical transport properties of LNO/STO (100) thin films.[13] Moreover, X-ray absorption measurements have demonstrated a modification of the Ni valence state at the interface to an STO substrate,[14] and resonant X-ray reflectivity data have shown a polarization of Ni *d*-orbitals at the interface to insulating $LaAlO_3$[15] has been performed. So far, however, little information is available on the atomic-resolution structure of LNO heterointerfaces and interfacial electronic structure change, particularly on STO substrate, which is required for a detailed interpretation of these results. On the other hand, as compared with other TMO interfaces, i.e., LAO ($LaAlO_3$)/STO interface, this specific interface is much less investigated. It would thus be very interesting to study the structural and electronic properties in such specific interface by means of modern HRTEM/STEM and EELS techniques in order to explore the unique properties.

II. EXPERIMENTAL DETAILS

The oxide multilayered heterointerface structure was grown on the (100) surface of STO by conventional pulsed laser deposition (PLD) with an oxygen background pressure of 0.5 millibars at a pyrometrically controlled temperature of 780 °C, as described elsewhere.[16,17] Cross-sectional TEM specimens were prepared using standard techniques. During the specimen preparation ethanol was used to avoid any contact of the specimen with water when grinding, dimpling, and polishing. The ion milling was conducted in a Fischione Ion Mill 1010 at 4.0 kV, 6.0 mA, and inclination angle of 10°. The TEM experiments were carried out using a 300 kV TEM (FEI Titan 80–300) with a field-emission gun and a spherical aberration corrector for the objective lens. The point-to-point resolution of the microscope is 0.78 Å for HRTEM and 1.35 Å for atomic resolution STEM at 300 kV. Atomic resolution STEM images were recorded using a HAADF (high-angle annular dark field) detector. The alignment of the C_S-corrector was done using the CEOS software based on aberration measurements deduced from the Zemlin tableau. Sufficiently small aberration coefficients were eventually achieved. All HRTEM images were recorded with small negative C_S ($-5.5\,\mu$m) and small higher-order aberration coefficients ($A3 \approx 1.0\,\mu$m, $S3 \approx 0.5\,\mu$m, and $A4 \approx 105\,\mu$m). A geometrical phase analysis[18,19] was used to probe the tiny variation in lattice plane spacing change and distortion across the interface.

High-resolution structural and electronic measurements were performed in a probe-corrected TEM/STEM system equipped with cold field-emission gun (JEOL JEM-ARM200CF), enabling sub-Å resolution in STEM imaging and spectroscopy. Atomically resolved STEM images were recorded using a HAADF detector. The EELS spectrometer (Gatan image filter Quantum ER imaging filter, with high-speed Dual EELS functions) provides an energy resolution of 0.3 eV and atomic-resolution spectroscopic imaging capability in cold-field emission gun (C-FEG) STEM. The probe convergence angle alpha was set to 25 mrad, corresponding to a probe size of ≈0.1 nm, and providing a probe current of 40 pA. Prior to the EELS quantification, the spectra were first processed by principal component analysis (PCA, a multivariate statistical analysis method), which is most helpful to reduce random noise from the spectrum image, and then quantification was performed. Acquisition time was set to 0.2 s for the Ti-$L_{2,3}$, O-K, La–$M_{4,5}$, and Ni-$L_{2,3}$ edges with a dispersion of 0.5 eV per channel. Measured elemental profiles for Ti, La, and Ti/O ratio across both interfaces were acquired by means of the MLLS (multiple linear least square) fit.

HRTEM image simulations were performed using JEMS software. The conditions selected according to the experimental conditions are: high voltage: 300 kV, C_S: $-10\,\mu$m, focus spread: 5.0 nm, specimen thickness: 1.6–3.3 nm, and defocus (over focus): 10.0–6.0 nm. Quantitative measurements of atomic position can be simply described in the following way. Based on the C_S-corrected HRTEM images, line-profiles across the interfaces were acquired. The atom column positions were carefully evaluated by a Pearson function fit to each maximum in line profiles extracted from the image, and then the accurate center position for each maximum as found by fitting is assigned as the center of atom column position. On this basis, atom column positions can be determined at a picometer precision.[4,5]

III. RESULTS

A. Orientation relationship

STO crystallizes in a cubic perovskite structure with lattice parameter $a = 0.3905$ nm. $LaNiO_3$ is rhombohedral with R-3c symmetry,[20] and the lattice constants $a = b = 0.54534$ nm, $c = 1.31369$ nm (indicated by the subscript "R"). The orientation relationship between rhombohedral LNO and cubic STO substrate are: LNO $[241]_R(1\bar{1}2)_R$//STO [100](001) and LNO $[110]_R(1\bar{1}2)_R$//STO [110] (001). Obviously, the NiO_6 octahedron exists within the unit cell. For simplicity, LNO is generally described in terms of a pseudocubic structure (indicated by the subscript "p") with a lattice constant of a = 0.3834 nm, for denoting the orientations and lattice parameter for LNO. The pseudocubic structure derived from rhombohedral LNO is defined as follows: LNO $[241]_R$, $[42\bar{1}]_R$, and $[\bar{2}2\bar{1}]_R$ corresponds to LNO $[100]_P$, $[010]_P$, and $[001]_P$, respectively. The angles in the pseudocubic structure are: 89.4°, 90.6°, and 89.4° between $[001]_P/[100]_P$, $[001]_P/[010]_P$, and $[100]_P/[010]_P$, respectively. With respect to STO, the lattice mismatch of pseudocubic LNO is −1.8%. The orientation relationship thus can be expressed as: LNO $[100]_p(001)_p$//STO [100] (001) and LNO $[110]_p(001)_p$//STO [110] (001). The angle between LNO $[100]_p$ and $[110]_p$ is 44.68°, which is smaller than 45° between [100] and [110] in the STO.

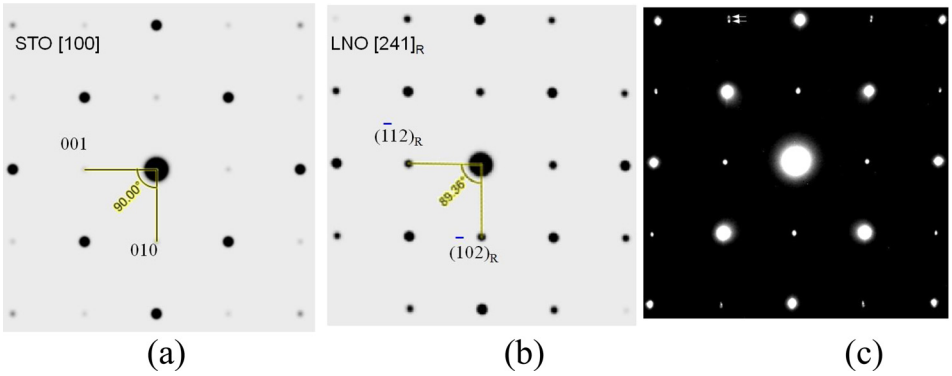

FIG. 1. The calculated diffraction patterns along STO [100] (a) and LNO $[241]_R$ (corresponding to pseudocubic $[100]_P$) (b). Electron diffraction pattern images from the LNO/STO bottom interface (c). Note that two sets of spots (indicated by arrows) which are originating from STO and LNO. The epitaxial relationship is clearly seen.

The orientation relationship is visualized in the diffraction patterns. The calculated diffraction patterns along [100] direction are shown in Figs. 1(a) and 1(b), where the angle and corresponding planes are clearly seen. It is noted that the corresponding weak reflections in STO should become stronger in LNO. Relevant information concerning the epitaxial relationship and the quality of layers is directly obtained from electron diffraction pattern from STO and LNO. Fig. 1(c) shows electron diffraction pattern recorded from the substrate STO including the thin LNO layer (around the bottom interface), which is a superposition from LNO layer and STO substrate. Due to a small difference in lattice constants, two sets of spots (indicated by arrows) are quite close. No other spots are observed due to the presence of other possible phases. The absolute intensity difference of weak spots in the pattern seems difficult to compare to the calculated patterns since the LNO layer contributing to selected area electron diffraction is only a very small portion in the cross-sectional view. Anyway, the electron diffraction pattern confirms the epitaxial relationship and layer quality.

B. Morphology of a trilayer structure

C_S-corrected HRTEM micrographs (Fig. 2(a)) and HAADF STEM image (Fig. 2(b)) taken along the [010] direction reveal that two heterostructure interfaces. Atomic columns at both "top" (STO-LNO) and "bottom" (LNO-STO) interfaces are resolvable. However, from the images, the bottom interface seems more atomically sharp than the top interface, which is clearly reflected in HAADF-STEM image. This implies that the intermixing occurs across the interface, which is proofed by the composition profiles. It is noted that numerous defects in the LNO layer emerge as "streak" features (labelled by white arrows). A STEM image more clearly sees the distribution and their morphologies of the defects in the layer. Actually, these defects are Ruddlesden-Propper (RP) faults both planar and in volume as reported by Detemple *et al.*[21] As a consequence of these faults, the appearance of multiple anti-phase regions exists. The RP faults can be easily seen in the HAADF image. Noticeably, the appearance of these anti-phase boundaries may modify the atomic stacking sequences, and then change the interface atomic terminating planes. It can be imagined that they should be linked to the interface polarities and the presence of interface atomic steps. On the other hand, these RP faults or anti-phase boundaries appear distinct features when viewed along [110] direction. They come out as many thin "lines" (not shown here) instead of "block" regions in [010] direction. These imply that the RP faults in LNO are two dimensional planar defects. Moreover, it is also seen that a defect free region exists at about 20 nm away from the bottom interface, and the interface is usually dislocation free. Such defect free region near the interface appears only when the film approaches a critical thickness, which mainly depends on the mismatch between the two lattices.

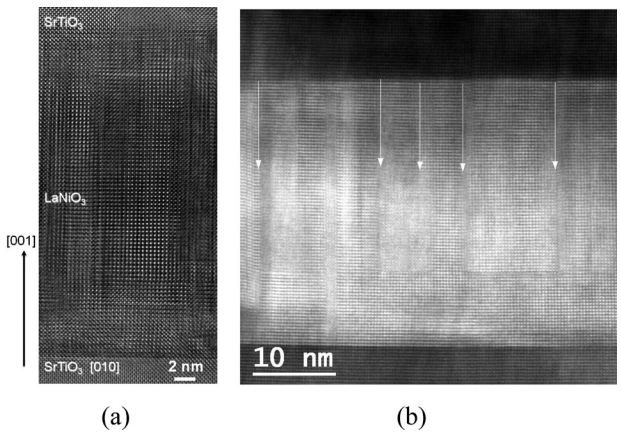

FIG. 2. (a) Cross-sectional C_S-corrected HRTEM image along [010] of the STO/LNO/STO heterostructure, consisting of the entire around 30.0 nm thick LNO layer and both interfaces. (b) High resolution STEM image clearly showing the respective layers.

HAADF STEM image (Fig. 2(b)) of the LNO layer taken from [010] direction gives much strong contrasts relative to STO. Since the intensity in HAADF image is approximately proportional to $Z^{1.7}$, from this direction the brightest spots in LNO correspond to the overlapping of lanthanum (57) and oxygen atoms and in STO to the overlapping of strontium (38) and oxygen atoms. According to the image contrast and the epitaxial relationship, it unambiguously concludes that bright Sr/La columns are directly faced to bright La/Sr columns at both interfaces, and moreover, the bottom and top interface show a distinct abruptness. However, to clearly determine the terminating atomic plane, atomic resolution imaging taken along [110] projection is essential.

C. Terminating atomic plane at bottom interface

To explore the interface-induced phenomena, the detailed atomic configurations need to be well clarified. To achieve this goal, the approach enabled by Cs-corrected atomic

resolution imaging and accompanied quantitative analysis is very essential. The atomic structure of the interface can be unambiguously identified based on the HRTEM image along [110] direction recorded under a negative C_S imaging condition,[22] as shown in Fig. 3, where individual atom column contrasts in STO and in LNO layers are clearly distinguishable. According to the atomic structure of LNO and STO, the octahedra in LNO rotate. Due to the rotation, O atomic columns in LNO are thus not exactly overlapping viewed from [110] projection. Through image calculations, which simulates the individual atom column contrast under the conditions equivalent to the experimental, the respective atom columns can be well discriminated. Two clippings of the calculated images (insets in Fig. 3(a)) are inserted into the experimental image, O, Ti, Ni, and SrO and LaO atom columns can be readily identified. These calculated images indicate that LaO and SrO columns appear as very strong bright dots whereas O, Ti, and Ni columns are imaged as weak dots under the experimental conditions. However, O atom intensities in LNO are relatively weak and "blurred" as compared to STO. Moreover, the O intensity difference between the calculated and experimental image seems somewhat higher than the La or Ni, which could be ascribed to the O easily loss under electron beam. The superimposed atomic models on the experimental image clearly designate all individual atom column arrangements along this projection. Careful examination of atom contrast changes at the interface (denoted by two separate rectangular dotted lines) further reveals the contrast difference at the interfacial plane from the left to right, especially the O atom column intensity difference. This suggests that at the interface one TiO atomic row in STO is likely linked to one NiO_2 row in LNO, creating an atomic-step. Two intensity traces acquired along the red (left part) and white (right part) lines (from C to D) perpendicular to interface are illustrated in Fig. 3(b), clearly indicating the intensity difference across the interface, which accordingly corroborates the presence of two different terminations at the examined location. The bottom interface seems a mixed interface, terminated by –LaO-TiO_2– or by –NiO_2-SrO–. Based on the above observations, two interfacial atomic models are thus proposed (Fig. 3(c)), which illustrate specific atomic configurations at the interface. Apparently, two distinct interfacial octahedra are formed and slightly deformed as compared to bulk, which can trigger an interfacial octahedron reconstruction[6] and subtle electronic changes locally.[23]

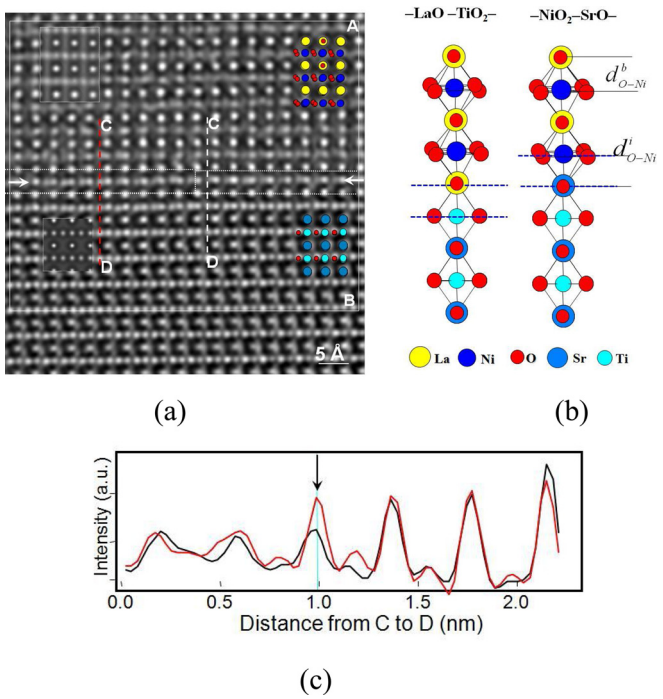

FIG. 3. (a) A portion of cross-sectional C_S-corrected HRTEM image (Wiener filtered) of bottom interface (LNO-STO) along STO [110], two clippings of the calculated bulk STO and LNO images based on the atomic models are superimposed on the experimental image. By comparing the intensity variation two distinct terminating configurations at the same interface are seen, as denoted by a dotted line. (b) Two corresponding atomic models and interfacial octahedra, i.e., -LaO-TiO_2- and –NiO_2-SrO-, respectively. (c) Two intensity traces acquired along the red (left part) and white (right part) lines (from C to D) reveal the intensity difference at the left and right part of the interface. The intensity trace (red) shows a remarkable high intensity compared to the black (corresponding to the white line). Black arrow indicates the intensity difference at corresponding interface locations. The interface is marked by white dotted lines in panel (a), and blue dotted lines in panel (b). Ni-O bond lengths at the interface and in bulk are indicated by d^i_{O-Ni} and d^b_{O-Ni}, respectively.

To prove the terminating plane, an atomic resolution HAADF STEM image along [110] was acquired (Fig. 4(a)). The brighter spots correspond to individual Lanthanum (57) and Strontium (38) atoms which are visible in LNO and STO. The weaker spots in between show Ti (22) and Ni (28) atom columns, whose intensities differ slightly because of a relatively small Z difference. This allows distinguishing LNO and from STO. All over the layers, the O contrasts are not visible under this condition. The HR-STEM image reveals that the interface is well defined. A corresponding intensity profile integrated over a rectangular area shows a clear jump (Fig. 4(b)) as crossing the interface from STO to LNO. The comparison of intensity shows that the interface is terminated by NiO_2 in LNO and SrO in STO. However, it is noticed that the intensity of NiO_2 terminating plane at the interface largely deviate from the bulk, which implies that to a certain extent the interfacial NiO_2 atomic plane is possibly partially mixed, i.e., with a TiO_2 layer, which is indeed consistent well with the preceding HRTEM observations. By closely examining the bottom interface over a large portion, we found that the bottom interface is predominantly terminated by –NiO_2-SrO–.

D. Terminating atomic plane at top interface

In the case of top interface (STO-LNO), from the HR-STEM image obtained along the [110] direction (Fig. 5(a)), where the difference of LNO and STO contrast is obvious, same as the bottom interface, the brightest and weaker dots corresponding to the atom column positions are well distinguishable, the interface location is well recognized. The interface position can be easily determined based on the intensity profile (Fig. 5(b)). According to the intensity traces across the interface, the LaO and TiO_2 columns at respective terminating planes at the interface are readily identified due to very pronounced intensity changes in comparison with the respective layer. At the interface, from LNO layer

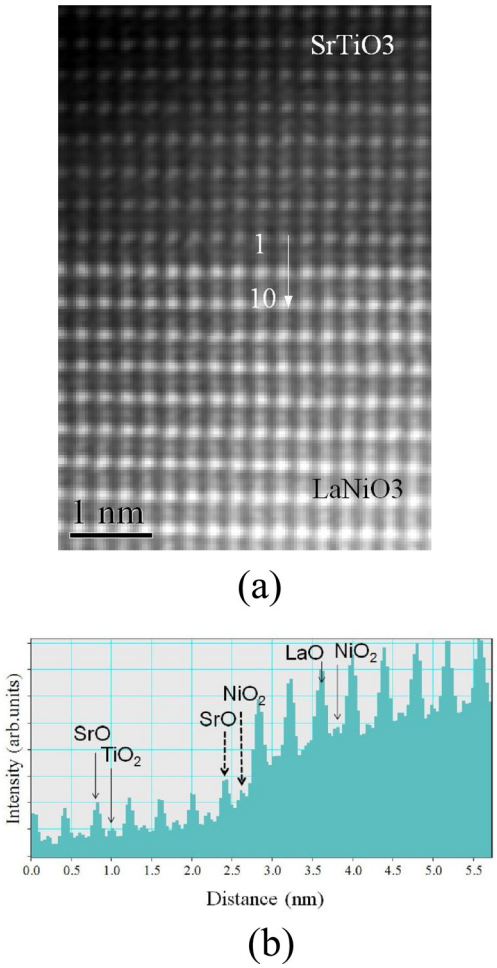

FIG. 4. (a) A HAADF-STEM image of bottom interface along STO [110], where the interface is quite obvious. (b) Line profiles of the image intensity across the interface. Note that bulk and interface terminating atomic planes are labeled by respective atomic planes. Interface atomic planes are highlighted by dashed lines.

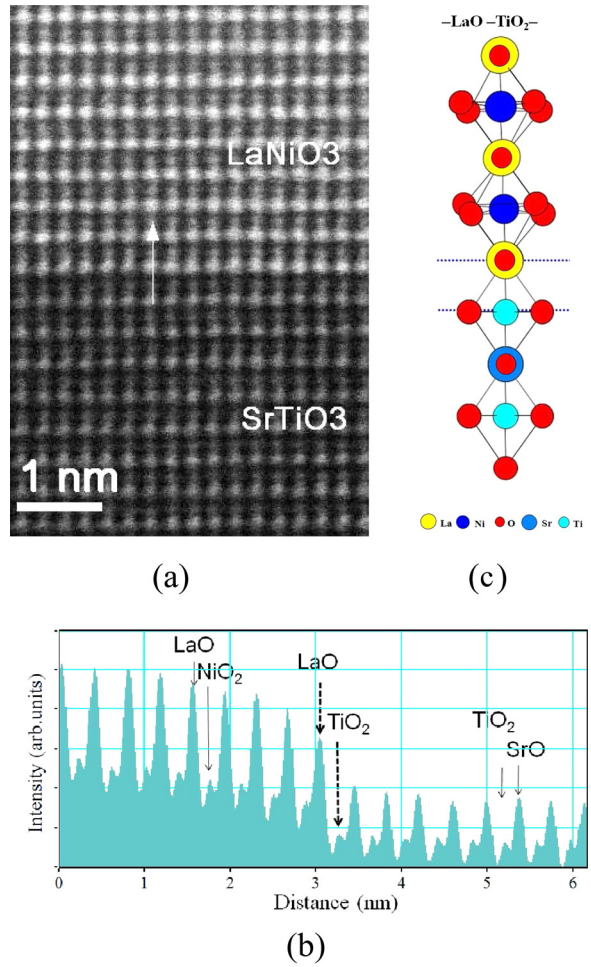

FIG. 5. (a) A HAADF-STEM image of top interface along STO [110]. (b) Line profiles of the image intensity across the interface, the terminating atomic planes. Note that bulk and interface terminating atomic planes are labeled by respective atom planes. Interface atomic planes are highlighted by dashed lines. (c) Possible interfacial octahedra structure, where interface atomic planes are indicated by dotted lines.

the interface is LaO-terminated, showing a strong contrast, whereas in STO it is TiO-terminated, showing a relative weak contrast. It is thus concluded that the top interface consists of $–TiO_2$-LaO–. Based on the atomic configurations, a corresponding octahedral structure at the interface is reconstructed (Fig. 5(c)). The O-Ti-O octahedron in the upper STO and the O-Ni-O octahedron in LNO are linked via sharing the O atom column in LaO plane. Evidently, two distorted interfacial octahedra are generated.

E. O-Ni bond length at the interface

To visualize the distorted octahedra at the interface, a HRTEM image taken from [110] direction (Fig. 3(a)) was utilized, thanks to the visibility of O atomic columns. Gaussian regress analysis was used to determine the atom column position by measuring the peak centre of the intensity profiles in picometer precision.[6,24] Here, the distorted octahedra in the $–NiO_2$-SrO- interface (bottom interface) were analysed. Owing to the shape of Ni-O octahedron at the interface, O-Ni bond length within an interfacial octahedron can be different in directions perpendicular or parallel to the interface.[25] By means of quantitative HRTEM, we are able to measure the tiny variation of O-Ni bond length (d) within the octahedra along the [001] direction, perpendicular to the interface ($d^i_\perp$), and along [-110] direction (in-plane), parallel to the interface ($d^i_{//}$). For comparison, the corresponding O-Ni bond length in bulk was also measured, labelled as $d^b_{//}$, $d^b_\perp$, respectively. The superscript b and i denote that the O-Ni bond length in bulk and at the interface, respectively (as shown in Fig. 3). Measured Ni-O bond length at the interface and in bulk are summarized in Table I.

It turns out that the averaged bond length at the interface given by $(d^i_\perp + d^i_{//})/2$, labelled by d^i_{O-Ni}, is (1.954 ± 0.158) Å while averaged value in bulk obtained by $(d^b_\perp + d^b_{//})/2$, labeled by d^b_{O-Ni}, is (1.938 ± 0.101) Å. The averaged elongation of Ni-O bond length at the interface is 0.016 Å. Moreover, the elongation of those Ni-O bond lengths, perpendicular to the interface, is 0.055 Å. Anyhow, the bond length of O-Ni at the interface is apparently increased with respect to the bulk. Interestingly, the measured Ni-O bond length in this work by quantitative HRTEM shows a reasonable agreement with the value measured by X-ray measurement,[26] which gives (1.968 ± 0.002) Å and (1.935 ± 0.002) Å for the interface and bulk, respectively.

TABLE I. Ni-O bond length at the interface and nearby bulk.

Notations	Ni-O bond length (Å)	Averaged Ni-O bond length	Methods
$d^i_{\perp}$	1.988 ± 0.034	1.954 ± 0.158	HRTEM[25]
$d^i_{//}$	1.920 ± 0.316		HRTEM
$d^b_{\perp}$	1.933 ± 0.034	1.938 ± 0.101	HRTEM
$d^b_{//}$	1.944 ± 0.201		HRTEM
$d^i_{\perp}$ (in-plane)	1.968 ± 0.002		XRD[26]
$d^b_{\perp}$ (out of plane)	1.935 ± 0.002		XRD[26]

The change of O-Ni bond length at the top interface (–TiO_2-LaO–) was also determined by applying similar technique. In Fig. 5(b), the spacing between two weaker peaks corresponds to two TiO_2 atomic planes in STO or two NiO_2 atomic planes in LNO. The measurement of the first NiO_6 octahedron next to the interface turns out that the O-Ni bond length is not significantly deviated from the bulk.

As shown above, the change of Ni-O bond length at two interfaces is obviously dissimilar. It markedly increases at the bottom interface while it shows no pronounced changes at the top interface. The physical mechanism for the change of Ni-O bond length is unclear. However, it may be rationalized simply by associating with the presence of oxygen vacancies at the interface. The presence of O vacancy slightly decreases the ionic Ni-O interaction, and on average decreases the bonding character. As a result, the elongation of the bond length of Ni-O is relatively small. For the bottom interface, where the Ni-O bonds are directly involved in forming the interfacial octahedra, it is thus strongly influenced by the presence of oxygen vacancies as compared with the top interface. On the other hand, as will be seen in the ensuing section, the first few atomic layers in LNO is fully strained on STO, which is not fully relaxed, regardless of the top and bottom interface. This implies that such interfacial effects might also contribute to an elongation of interfacial Ni-O bond lengths we measured.

F. Atomic displacements and lattice distortions

Interfacial structure variations can be demonstrated in the change of atomic displacement crossing the interface. Using the geometrical phase analysis,[18,19] the $d_{(001)}$ interplanar spacing was determined across both interfaces (Fig. 6, {100} cross section). In fact, the $d_{(001)}$ spacing corresponds to a length of one TiO_6 or NiO_6 octahedron in the direction perpendicular to the interface, or along the growth direction. From (001) spacing profile, we found lattice dilation at both interfaces along the growth direction. The measurements carried out from {110} cross section also shows lattice dilation at both interfaces (not shown here).

To further examine structural distortions at the interfaces, here, the evolution of the ratio, $(c/a)_{STO}$ and $(c/a)_{LNO}$, is further derived as a function of (001) atomic plane number (or unit cell number), where a and c are the bulk lattice constants along [100] and [001] directions, respectively. The ratio is obtained by using atomic displacement divided by 0.3905 for STO, and 0.3834 for LNO (note that the (c/a) ratio at the interfaces is obtained using a_{STO} bulk value). At two interfaces, the ratio evolution (c/a) extending into 14 atomic planes on both sides from interface is plotted in Fig. 6. The plot clearly shows that: (i) the first 1–5 atomic planes are strongly affected by interface, and ratio changes are more pronounced when crossing the interface; (ii) the ratio change is stronger in LNO than STO; and (iii) the ratio evolution at both interfaces are slightly different. Furthermore, the maximum ratio is $(c/a) = 1.025$ in LNO. It also indicates that the first few unit cells in LNO are fully strained on STO. However, with increasing atomic layers in the LNO layer structural relaxation occurs, the (c/a) ratio nearly approaches a constant value. To some extent, such ratio evolution can reflect the interfacial relaxation effect, implying how the atomic distance be modified due to the presence of interface elastic mismatch. From the image, no dislocations or other defects near the interfaces could be seen until the twins or RP faults in LNO (a few nanometers away from interface) appear. This means the structural relaxation effects at the interface hardly start within a few nanometers from interfaces, which is exactly reflected in the ratio (c/a) change. In other words, the measurement of the (c/a) ratio may cast light on the interface structural relaxation effects. It is also interestingly noted that the ratio change in STO at the top interface seems more pronounced than bottom interface. As will be seen, the Ti-$L_{2,3}$ fine structure at the top interface shows a more significant change (see Fig. 7(b)), which is intrinsically structure-relevant.

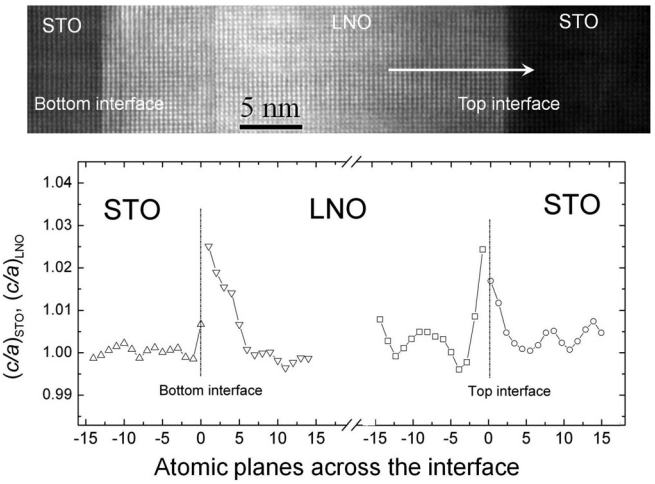

FIG. 6. A segment of HR-STEM image along STO [010], and below is the ratio evolution of (c/a) in STO and LNO across the interfaces which is extended into 14 atomic planes on both sides from the interface. The interface locations are indicated by dotted lines. The arrow indicates the growth direction [001].

G. Electronic structures at the interface

1. Ti-$L_{2,3}$ edge

The electronic structures at both interfaces are probed by EELS analysis in STEM. Step scanning was acquired using a probe of 0.95 Å, and a step width of 1.0 Å. Extraction of unambiguous Ni-$L_{2,3}$ signals is hampered by severe overlap with the La-$M_{4,5}$ edge. Therefore, changes in Ti-$L_{2,3}$

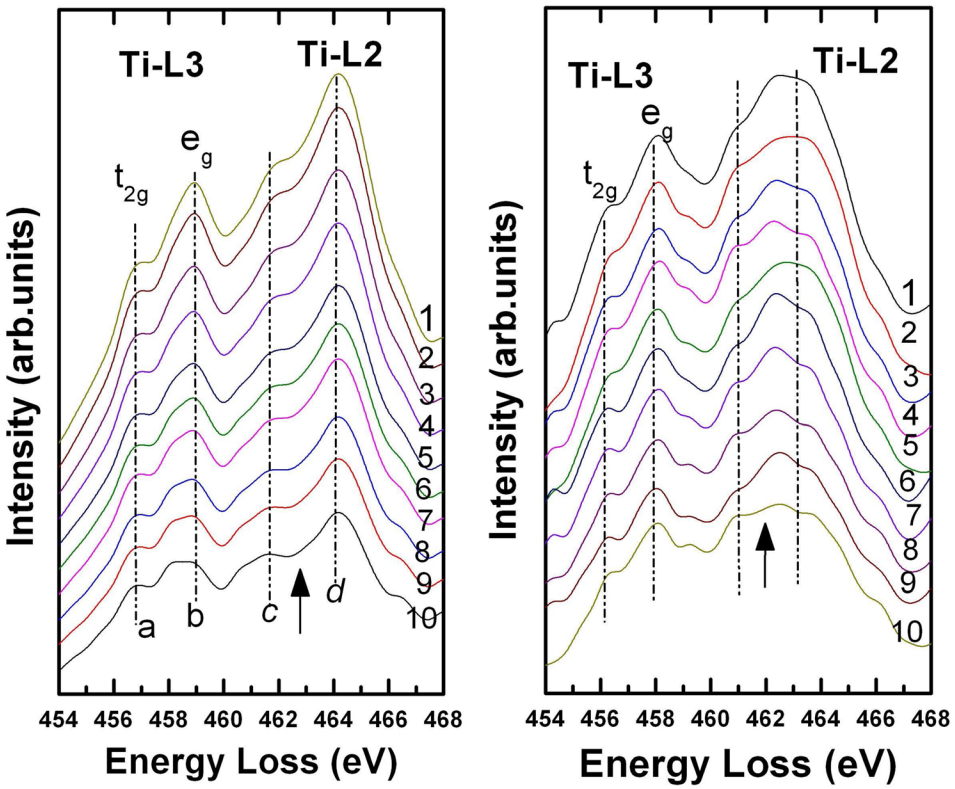

FIG. 7. (a) A series of Ti-$L_{2,3}$ spectra across the interface recorded from bottom interface along the direction labeled by an arrow in Fig. 4(a). (b) A series of Ti-$L_{2,3}$ spectra across the interface along the line labeled in Fig. 5(a). Spectra were recorded at an interval of every 1.0 Å across the interface. The valley (e_g and t_{2g}) in Ti L_2 is indicated by arrows, and note that the changes and the difference between the present Ti-L_2 with the Ti $2p$ x-ray-absorption spectra in Ref. 32.

ELNES (energy-loss near edge structure) are closely examined by acquiring a series of spectra across the interface (Fig. 7). Ti-$L_{2,3}$ edge consists of four peaks, labeled as a, b, c, and d, which are attributed to the transitions from Ti-$2p$ to Ti-$3d$ levels, corresponds to $2p_{3/2} \rightarrow 3d_{t_{2g}}$, $2p_{3/2} \rightarrow 3d_{e_g}$, $2p_{1/2} \rightarrow 3d_{t_{2g}}$, and $2p_{1/2} \rightarrow 3d_{e_g}$, respectively. EELS-line scan was performed along [110] STO direction (shown in Fig. 4(a), a segment of bottom interface HAADF-STEM image). Series of Ti-$L_{2,3}$ spectra across the bottom interface are shown in Fig. 7(a). Detailed analysis of these spectra recorded at 1 Å spatial resolution reveals that approaching to the interface the Ti-L_3 splitting becomes smaller than in the STO layer. A gradually broadening and reduced intensity in the L_3-e_g level are observed when moving from STO to the interface. It may imply the presence of distorted TiO_6 octahedra at or adjacent to the interface.

The same EELS measurements were performed on the top interface. A series of Ti-$L_{2,3}$ spectra (Fig. 7(b)) were recorded within a range of about 1.0 nm across the interface along [110] STO (indicated in corresponding STEM image, Fig. 5(a)). It is clearly seen that with respect to the bottom interface, the main difference in the fine structures of Ti-$L_{2,3}$ at the top interface is L_2 edge, not L_3 edge. The L_2-e_g edge is gradually reduced as crossing the interface whereas the L_3 edge shows no pronounced change except a very small reduction in the intensity of L_3-e_g. Close examination and comparison between the fine structures obtained from both interfaces reveal the electronic structures are different. Such subtleties are essentially attributed to the dissimilarity of intrinsic atomic structure at both interfaces. Relatively, the remarkable change of Ti-$L_{2,3}$ fine structure at the top interface also corroborates that the Ti-O bonds are directly involved in forming an interfacial octahedral as revealed by HRTEM qualitative analysis in Fig. 5 and the (c/a) ratio evolution in Fig. 6. Furthermore, it is seen in Sec. III G 2 that the subtleties in Ti-$L_{2,3}$ could also link to the charge transfer at two interfaces.

2. O-K edge

EELS spectra of O-K edge acquired from STO, at both interfaces as well as LNO layer, each was summed over 10 spectra within 5 Å range from the bulk or crossing the interface, are shown in Fig. 8. The ELNES structure of the O-K edge is usually governed by the hybridization of $2p$ anion states with $3d$ metal states, forming empty bands of predominantly metal character above the Femi level.[27] Despite the noisy of the spectra, the main features are clearly visible. Three distinguished peaks indicated by short dotted lines are essentially attributed to the different orbit-orbit interactions; the peak intensity, and relative position for these peaks are different at the interface region and in the respective STO and LNO layers. The difference in the O-K edge fine structure between bottom and top interface is quite apparent, which is mainly reflected in the second peak. The O-K fine structures at the bottom interface are quite similar to STO bulk spectrum, while one at the top interface is unlike neither STO nor LNO. Considering the changes displayed in Fig. 8, there seems to be a continuous variation at the bottom interface from substrate STO to LNO layer, whereas it is not the case at the top interface from LNO to top STO.

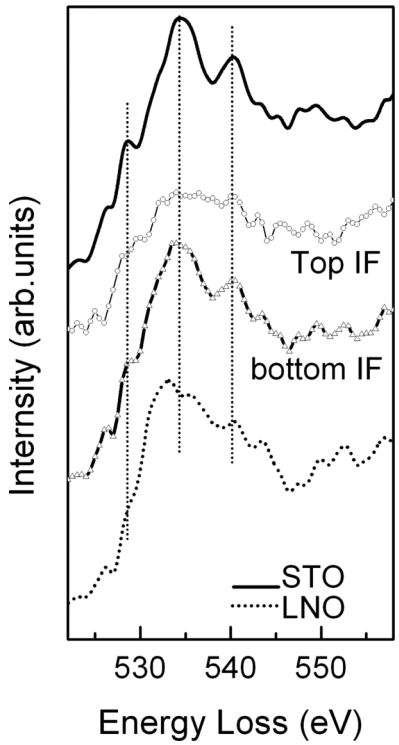

FIG. 8. The O-K edges obtained from the bottom and top interface regions, and nearby bulk STO and LNO.

H. Atomic ratio at the interface

To have the elemental information at or adjacent to the interface, the relative chemical composition profiles of La and Ti atom across both interfaces were acquired by EELS quantification as shown in Fig. 8. From the plot, it is seen that at two interfaces, a gradient variation of La and Ti nearly within one unit-cell exists. However, the change of La and Ti at the bottom interface is abrupt than at the top interface (Fig. 9). It is consistent with the observations of contrast variations in the STEM image, where the intensity profile at the bottom interface is sharper than at the top interface (Figs. 4(a) and 5(a)). This could imply that the interdiffusion at the top interface is much pronounced that at the bottom interface, particularly, La elements. The measurement uncovers that a certain amount of chemical intermixing of La or Ti took place during the growth process, but with a different degree of intermixing at both interfaces thanks to the grown conditions.

Moreover, much attention has also been paid to detect the change of Ti/O ratio as O vacancies play an important role in interface polarity and oxide interface engineering. The ratio change is shown at the bottom of the plot. Interesting to note that at the interface locations, the exact Ti/O ratio somewhat deviates from the nearby STO bulk value and extends into the LNO layer. It is less than the bulk Ti/O ratio (0.33) at the interface. This is an evidence demonstrating a non-stoichiometric chemistry at the interface and adjacent to the interface. Further scrutiny shows that there is a tiny jump of Ti/O ratio at the top interface in contrast to a continuous change at the bottom interface although both present a similar varying tendency. The non-stoichiometric chemistry could manifest a certain amount of oxygen vacancies possibly prevailing at both interfaces.

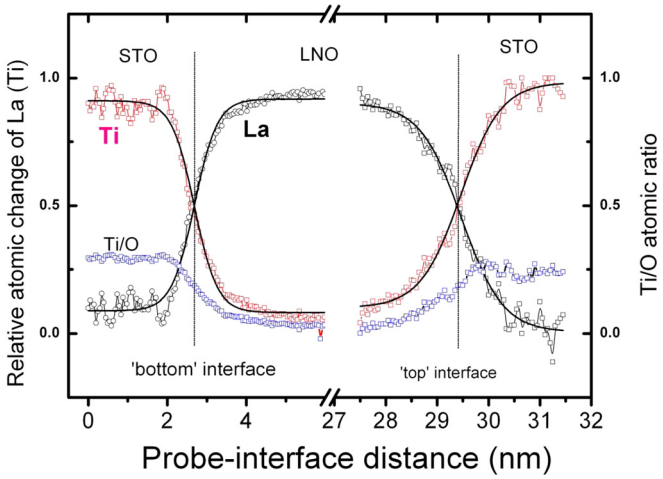

FIG. 9. The normalized relative atomic distributions of La (containing a small amount of Ni signals), Ti as well as the Ti/O atomic ratio across both interfaces are shown, where the nonlinear curves are obtained by fitting the data to a Boltzman function. Two interface locations are labeled by two lines.

IV. DISCUSSION

From the detailed structural analysis, it is known that bottom interface is –SrO-NiO_2– terminated while the top interface is –TiO_2-LaO– terminated. Forming a dissimilar interface at the bottom and top could be due to the energetic reasons during the film growth. The same interface configurations at the top and bottom will lead to a non-stoichiometric interlayer, which hardly minimize the system energy. It can be imagined that the terminating planes can be controlled by manipulating the deposition conditions.

With the structural analysis and EELS/ELNES measurements, here, we can further discuss the intrinsic phenomenon triggered by the terminating atomic planes. Both are polar interfaces. The polar layers (LaO and NiO_2) on the nonpolar STO lead to the appearance of polar mismatch. Such polar misfit will cause the interface unstable. From STO to LNO, and from LNO to STO, a polar discontinuity is present at both interfaces. Such polar discontinuity is similar to the interface of LAO/STO heavily studied recently. To stabilize the polar discontinuity, several mechanisms, such as electronic reconstruction model,[28,29] oxygen vacancy,[23,30] and lattice strains,[31] were suggested to explain the experimental details in LAO/STO system. For the LNO/STO, the lattice distortions at the interface regions as measured from the atomic displacement and (c/a) ratio change are quite pronounced at both interfaces, which are confirmed by measurements in both {100} and {110} cross sections. It implies that the lattice distortions may be intrinsic present at the LNO/STO interface although a slight different magnitude at the bottom and top interface. Considering the polar character at the interfaces, the presence of atomic displacement-controlled lattice distortion at interfaces partially compensates the polar discontinuity. Apart from the lattice distortions, the charge transfer most likely occurs at the interface, yielding a reduction of Ti valency, further compensating the polar discontinuity. This is

indeed reflected in a series of EELS measurements on the Ti-$L_{2,3}$ fine structures.

From the EELS spectra measurements, we noted only a small change of Ti-$L_{2,3}$ edge at/near the bottom interface whereas a larger change exists at the top interface. This indicates the absence of strong valence effects in the bottom interface and likely presence of strong valence effects in the top interface. For simple interpretation, we compare our Ti-$L_{2,3}$ EELS edge at both interfaces with X-ray absorption spectroscopy (XAS) obtained from Abbate *et al.* (Figure 1 in Ref. 32, Ti 2p x-ray-absorption spectra of La_{1-x} Sr_x TiO_3 as a function of Sr content). From the reference spectra in Ref. 32, one can estimate the valency of Ti by comparing the shape of Ti-$L_{2,3}$ edge. The valley between two peaks (e_g and t_{2g}) in L_2 edge is changed with Ti valency, as shown, the depth of this valley reduces up to $x = 0.8$. A shift of valence towards 3+ will show as a progressive fading of these peaks and an increase of signal in the valley in between (Figure 1 in Ref. 32).[23,33] By comparison, we are able to estimate the Ti valency from EELS spectra to be at least $Ti^{>3.8+}$ ($x \geq 0.8$) at the bottom interface whereas it is in the range of $Ti^{3.4+} \sim Ti^{3.0+}$ ($0.4 \geq x \geq 0$) at the top interface. It is clearly seen that bottom and top interfaces have different Ti valency. This is a clear indication for charge transfer located at Ti sites. It also means a different amount of charge transfer at both interfaces has occurred. Interestingly, at the top interface (–TiO_2-LaO–), Ti valency is close to Ti^{3+}, the bare STO substrate does not show any $Ti^{3.0+}$, thus also indicating that the LNO/STO interface is important to collect the mobile amount of electrons. Note that the top interface remarkably show a bigger change in Ti-$L_{2,3}$ fine structure, which may be also relevant to the terminating atomic planes, where a TiO_2 is directly involved in forming the interfacial octahedral, in contrast to the bottom interface (–SrO-NiO_2–). However, our finding seems different from the observations in STO-LAO interface,[29] indicating that the *p*-type interface (SrO-terminated STO substrate) displays a bigger charge in Ti-$L_{2,3}$ edge. In sum, ELNES analysis reveals a valency change of Ti at/adjacent to the interface. According to ELNES analysis and the discussions given above, we may draw a reasonable conclusion that the polar discontinuity at the interfaces is possibly compensated by the charge transfer.

Taken together, possibly, two mechanisms, lattice distortions and charge transfer at the interfaces, are mainly responsible for compensating the polar discontinuity at the LNO/STO interface. However, it must be pointed out that the presence of oxygen vacancies, chemical intermixing can also play a significant role on the polar discontinuity at the interface.[30,33] The correlations between interfacial polarities with these effects need further experimental study and theoretical supports with the *ab-initio* calculations.

V. SUMMARY

To summarize, an extensive characterization of atomic and electronic structures at the STO/LNO/STO heterointerfaces was carried out by a combination of aberration-corrected high-resolution TEM and STEM, and electron diffraction pattern. Combined with the detailed quantitative image and spectrum analysis, the interfacial atomic and electronic structures are revealed. At the top interface (STO-LNO), the atomic stacking sequence is –TiO_2-LaO–, where the TiO_2 is directly coupled with the LaO layer in LNO. The bottom interface is predominantly –NiO_2-SrO– terminated. The Ni-O bond lengths at both interfaces are experimentally determined which shows a remarkable increase at the bottom interface (LNO-STO) whereas it shows a minor increment at the top interface. Atomic displacement across the interface shows an elongation of the interfacial octahedral, and lattice distortions is more obvious in LNO layer than in STO. Atomic resolution EELS analysis on the Ti-$L_{2,3}$ fine structure reveals that the electronic structure changes at the bottom and top interfaces are dissimilar. It also coincides with the quantitative atomic structure observations that are associated with non-identical terminating atomic planes. According to the EELS measurements and interfacial structural distortion analysis, the interfacial polar discontinuity and charge transfer are discussed, indicating a different charge state at the two interfaces.

ACKNOWLEDGMENTS

Gabriele Moser and Herwig Felber are gratefully acknowledged for their help with the sample preparation.

[1]For a review, see M. Imada, A. Fujimori, and Y. Tokura, Rev. Mod. Phys. **70**, 1039 (1998).
[2]J. Mannhart and D. G. Schlom, Science **327**, 1607 (2010).
[3]P. R. Willmott *et al.*, Phys. Rev. Lett. **99**, 155502 (2007).
[4]K. Urban, Science **321**, 506 (2008).
[5]A. Y. Borisevich *et al.*, Phys. Rev. Lett. **105**, 087204 (2010).
[6]C. L. Jia, S. B. Mi, M. Faley, U. Poppe, J. Schubert, and K. Urban, Phys. Rev. B **79**, 081405R (2009).
[7]J. Chaloupka and G. Khaliullin, Phys. Rev. Lett. **100**, 016404 (2008).
[8]P. Hansmann *et al.*, Phys. Rev. Lett. **103**, 016401 (2009).
[9]G. Giovannetti *et al.*, Phys. Rev. Lett. **103**, 156401 (2009).
[10]S. J. May, T. S. Santos, and A. Bhattacharya, Phys. Rev. B **79**, 115127 (2009).
[11]R. Scherwitzl *et al.*, Appl. Phys. Lett. **95**, 222114 (2009).
[12]J. Son *et al.*, Appl. Phys. Lett. **96**, 062114 (2010).
[13]G. P. Mambrini *et al.*, J. Appl. Phys. **102**, 043708 (2007).
[14]J. Liu *et al.*, Appl. Phys. Lett. **96**, 133111 (2010).
[15]E. Benckiser *et al.*, Nature Mater. **10**, 189–193 (2011).
[16]T. Holden, H.-U. Habermeier, G. Cristiani, A. Golnik, A. Boris, A. Pimenov, J. Humlicek, O. I. Lebedev, G. Van Tendeloo, B. Keimer, and C. Bernhard, Phys. Rev. B **69**, 64505 (2004).
[17]H.-U. Habermeier, G. Cristiani, R. K. Kremer, O. Lebedev, and G. Van Tendeloo, Physica C **364**, 298 (2001).
[18]K. Gutakovskii, A. L. Chuvilin, and S. A. Song, Bull. Russ. Acad. Sci.: Phys. **71**, 1426 (2007).
[19]M. J. Hytch, E. Snoeck, and R. Kilaas, Ultramicroscopy **74**, 131 (1998).
[20]J.-C. Park, D.-K. Kim, S. H. Byeon, and D. Kim, J. Synchrotron Radiat. **8**, 704 (2001).
[21]E. Detemple *et al.*, J. Appl. Phys. **112**, 013509 (2012).
[22]C. L. Jia, M. Lentzen, and K. Urban, Science **299**, 870 (2003).
[23]J.-L. Maurice, G. Herranz, C. Colliex, I. Devos, C. Carretero, A. Barthelemy, K. Bouzehouane, S. Fusil, D. Imhoff, E. Jacquet, F. Jomard, D. Ballutaud, and M. Basletic, Europhys. Lett. **82**, 17003 (2008).
[24]L. Houben, A. Thust, and K. Urban, Ultramicroscopy **106**, 200 (2006).
[25]Since the projection of the NiO_6 octahedra can be clearly seen in the HRTEM image along [110], we decompose the Ni-O bond length into two components: one is perpendicular to the interface and the second part is parallel to the interface. All Ni-O bond lengths in bulk and at the interface are composed of these two components. The averaged bond lengths of two components are assigned to the final Ni-O bond length at the interface or in bulk. The standard deviation of statistical measurements is set as an error bar.

[26]S. J. May, J.-W. Kim, J. M. Rondinelli, E. Karapetrova, N. A. Spaldin, A. Bhattacharya, and P. J. Ryan, Phys. Rev. B **82**, 014110 (2010).
[27]M. Abbate *et al*., Phys. Rev. B **46**, 4511 (1992).
[28]N. Nakagawa, H. Y. Hwang, and D. Muller, Nature Mater. **5**, 204 (2006).
[29]J. Verbeeck *et al*., Phys. Rev. B **81**, 085113 (2010).
[30]A. Brinkman *et al*., Nature Mater. **6**, 493 (2007).
[31]R. Pentcheva and W. E. Pickett, Phys. Rev. Lett. **102**, 107602 (2009).
[32]M. Abbate *et al*., Phys. Rev. B **44**, 5419 (1991).
[33]J.-L. Maurice, D. Imhoff, J.-P. Contour, and C. Colliex, Philos. Mag. **86**, 2127 (2006).